COBEM 2023 27TH INTERNATIONAL CONGRESS OF MECHANICAL ENGINEERING

ABCM Brazilian Society of Mechanical Sciences and Engineering
27th ABCM International Congress of Mechanical Engineering
December 04-08, 2023, Florianópolis-SC, Brazil

COB-2023-1426
OPTIMAL PREPROCESSING FOR PROPER ORTHOGONAL DECOMPOSITION OF THE OSCILLATORY METHANE JET DIFFUSION FLAMES DATASET

Fernanda Spilotros Costa Cordeiro
Leonardo Santos de Brito Alves
Davi Saadi de Almeida Lettieri
Departamento de Engenharia Mecânica, Universidade Federal Fluminense, Rua Passo da Pátria 156, Bloco E, sala 211, Niterói, RJ, 24210-240, Brazil.
fernandacordeiro@id.uff.br, lsbalves@id.uff.br, davilettieri@id.uff.br

Abstract. *This study aims to establish an optimal image processing for images from the oscillatory methane jet diffusion flames experiment and its impact on proper orthogonal decomposition (POD). Modal decomposition techniques arewidely used to characterize the behavior of unsteady dynamical systems. They provide a systematic way to generate low-dimensional approximations of a large set of high-dimensional dynamical systems. In order to reduce the order of the dynamic system that models oscillatory diffusion flames, it is necessary to topologically analyze the trajectories of the POD coefficients by means of their phase portraits. However, since the input data are images from the experiment, the signal-to-noise ratio can be quite high. Hence, filtering techniques employed on images allow the extraction and identification of essential elements of the images, and improve the visual quality of certain structural aspects, facilitatingtheir computational interpretation. In this paper, we present the image processing techniques known as median filter, block-matching and 3D filtering (BM3D) and threshold filter, which aims to remove as much noise as possible from the original data. The removal of noisy signals through such processing is fundamental for the accurate generation of higher-order POD coefficients. Based on this statement, several filtering parameters were tested on the images from the flamesexperiment, generating the phase portraits obtained from the POD decomposition. The obtained results were compared with each other to evaluate which parameter provides the highest number of accurate POD coefficients.*

Keywords: *Proper Orthogonal Decomposition (POD), Image Processing, Signal-to-Noise Ratio, Phase Portraits*

1. INTRODUCTION

Modal decomposition techniques have an extensive history of development throughout the 20th century. The understanding of vibration modes and their effects on structural analysis have been significant for the advancement of research, as they have played a fundamental role in analyzing the dynamic behavior of structures and their response to the dominant mode of vibration. Normally, the space-time relationship has complex dynamics and is modeled using partial differential equations. In this situation, the use of proper orthogonal decomposition (POD) is convenient (Lumley, 1967). This modal decomposition technique extracts the dominant modes of vibration in relation to the energy content. However, POD is very vulnerable to noisy data, which can be captured during the oscillatory diffusion flames experiment. As a consequence, the dominant modes and their phase portraits can be affected. In order to overcome these difficulties, image processing techniques are being implemented prior to the modal decompositions. This enables the existing noise to be reduced before actually evaluating the dominant modes and their phase portraits of the POD decomposition. The area of noise filtering is an important tool in many research projects, as it allows the use of input data with refinement in terms of discrepant data. One of the most widely used image processing methods is known as the median filter. It is a non-linear signal processing method, which introduced the idea of using the median to smooth impulse noise in digital images (Lee, 1980). In unidimensional terms, the median filter consists of a moving window covering an odd number of pixels. The value of the central pixel of the window is replaced by the value of the median of the pixels in the moving window (Tukey, 1971). The most notable advantage of the median filter is that it preserves characteristics of the original image, such as edges and relevant details, while at the same time it reduces noisy signals. Another widely used filter is known as BM3D (**B**lock-**M**atching and **3D** filtering), which is based on grouping of similar pixels in a digital image, in which filtering extracts redundancies to remove noise through **M**ean **S**quare **E**rror (MSE) (Dabov et al., 2007). In situations involving low-light experimental images, noise becomes a significant problem, as it generates dark, grainy images with very few details. In these cases, the BM3D filter is indicated to reduce noise in experimental images, as it can more efficiently refine the resulting quality of the dark experimental image. Lastly, the threshold filter is a technique that originates from the earliest image processing and is used in studies to binarize an image based on a specific threshold value. This filter highlights edges and contours, which makes the objects of interest stand out from the background. Therefore, the thresh-

old filter simplifies the image by highlighting the regions of interest, which meet the color or intensity criteria. In this filtering, the values of each pixel are compared with the threshold value, which assigns a new value to the pixel, which will become white or black. In other words, a binary value is assigned to each pixel that was previously at various levels of intensity, usually 0 (black) to 255 (white) (Parker, 2011).

Therefore, in this paper, the median, BM3D and threshold filters will be applied to the images obtained from the oscillatory methane jet diffusion flames experiment, in order to reduce the noisy data to a minimum. The filtered images will then serve as input data for the POD decomposition, which will generate the most energetic dominant modes and their respective phase portraits. The filtering parameters will be analyzed and discussed throughout this paper, which will determine the optimal set of denoising parameters.

2. MATHEMATICAL FORMULATION

2.1 Image Processing

2.1.1 Median Filter

The median filter manipulates a gray-scale digital image in which the pixels are localized by a coordinate (x, y). The neighborhood of each pixel is defined by a moving window of integer size $N \times N$. The values of the neighboring pixels are collected and arranged in ascending order. Finally, the median is calculated as the value of the pixel that occupies the central position of the sorted set. The value of the pixel processed by the median filter at position (x, y) is given by:

$$\mathbf{p}_{med}(x, y) = \mathbf{median}[\mathbf{p}(x', y')] \,, \tag{1}$$

where $\mathbf{p}_{med}(x, y)$ is the value of the pixel processed by the median filter at position (x, y) and $\mathbf{median}[\mathbf{p}(x', y')]$ is the median value of the neighboring pixels at position (x', y').

2.1.2 Block-Matching and 3D Filtering

The BM3D filter can be mathematically summarized in 6 general steps (Dabov et al., 2009). The first stage of the algorithm consists of dividing the original digital image into non-overlapping blocks. In the second step, for each divided block, the block matching process is carried out on a search area in the image, with the aim of finding blocks that are similar to each other. This can be done using the **M**ean **S**quare **E**rror (MSE). Once the blocks are similar, the third stage begins, which groups them into blocks that share similar visual characteristics. Moving on to the fourth stage, for each grouping of blocks formed, a set of parameters used to model the noise present in the blocks is estimated, such as the filtering intensity. In other words, the filtering intensity parameter indicates the filtering power that will be applied to each block grouping. In this sense, the higher the filtering intensity parameter, the greater the amount of noise eliminated. In the fifth step, the filtered blocks are aggregated and form the restored digital image, taking into account the overlap between the blocks and applying a weighted average to obtain the restored digital image. Finally, the sixth step is optional, but is commonly employed in a variety of situations. In this step, a post-processing is performed to further refine the quality of the restored digital image, which includes contrast adjustments, detail enhancement, sharpness, among others. The following figure exemplifies the 6 general commented steps of the BM3D filter.

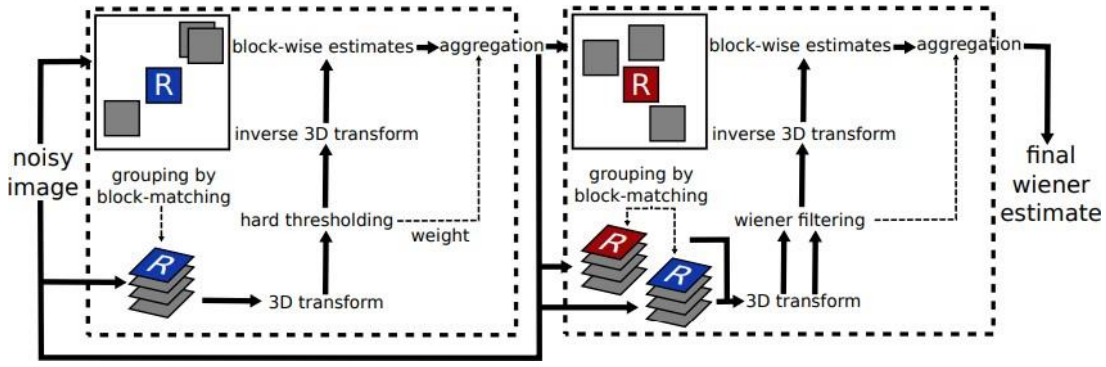

Figure 1. Schematic implementation of the BM3D filter. Image extracted from the paper of LeBrun, 2012.

2.1.3 Threshold Filter

For the threshold filter, it is necessary to highlight the objects of interest from the background. Therefore, the segregation of objects and background occurs through a threshold value T, which segments the image in respect of the two-dimensional intensity characteristics. Consequently, for any pair of coordinates $(x.y)$, the image processed by the threshold filter is defined as:

$$g(x,y) = \begin{cases} \text{object}, & f(x.y) > T \\ \text{background}, & f(x.y) > T \end{cases}, \tag{2}$$

where $f(x.y)$ is the two-dimensional function of the digital image, T is the value of the threshold filter and $g(x,y)$ is the function of the processed image.

2.2 Proper Orthogonal Decomposition

We will consider any large set of data, which are placed in a matrix $\mathbf{X} \in \mathbf{C}^{n\times m}$:

$$\mathbf{X} = \begin{bmatrix} | & | & | & | \\ x_1 & x_2 & \cdots & x_m \\ | & | & | & | \end{bmatrix} \tag{3}$$

where the columns $x_m \in \mathbf{C}^{n\times m}$ are input data, which can be obtained from experimental data, spatial or temporal data, sensing data or numerical simulation data.

The matrix decomposition known as **S**ingular **V**alue **D**ecomposition (SVD) is a single matrix decomposition of data, which can be represented as:

$$\mathbf{X} = \mathbf{U}\Sigma\mathbf{V}^T \tag{4}$$

$$\mathbf{X} = \begin{bmatrix} u_{11} & u_{12} & \cdots & u_{1n} \\ u_{21} & u_{22} & \cdots & u_{2n} \\ u_{31} & u_{32} & \cdots & u_{3n} \\ \vdots & \vdots & \ddots & \vdots \\ u_{n1} & u_{n2} & \cdots & u_{nn} \end{bmatrix} \begin{bmatrix} \sigma_1 & 0 & \cdots & 0 \\ 0 & \sigma_2 & \cdots & 0 \\ \vdots & \vdots & \ddots & \vdots \\ 0 & 0 & \cdots & \sigma_n \end{bmatrix} \begin{bmatrix} v_{11} & v_{12} & v_{13} & \cdots & v_{1m} \\ v_{21} & v_{22} & v_{23} & \cdots & v_{2m} \\ \vdots & \vdots & \ddots & \ddots & \vdots \\ v_{m1} & v_{m2} & v_{m3} & \cdots & v_{mm} \end{bmatrix}^T \tag{5}$$

where the orthogonal columns belong to the unitary matrices $\mathbf{U} \in \mathbf{C}^{n\times n}$ and $\mathbf{V^T} \in \mathbf{C}^{m\times m}$. The central matrix belongs to $\mathbf{R}^{n\times m}$, and is symbolized by Σ. Moreover, the matrix Σ is non-negative on the diagonal entries and zero off the diagonal, representing the singular values of the decomposition.

The POD decomposition is also known as the SVD applied to **P**artial **D**ifferential **E**quations (PDE). Therefore, any PDE can be defined as follows:

$$u_t = N(u, u_x, u_{xx}, \cdots, x, t) \tag{6}$$

where the subscripts x and t denote partial differentiation and N represents the spatial-temporal dynamics, which is the nonlinear evolution.

There are several methods that solve a PDE. Among them, there are the methods of separation of variables and orthogonal basis expansion. Using such methods, the solution of the PDE can be represented as:

$$u(x,t) = \sum_{n=1}^{N} a_n(t)\phi_n(x) \tag{7}$$

where $\phi_n(x)$ are the orthogonal eigenvectors, known as basis functions, and $a_n(t)$ are the temporal coefficients related to the temporal dynamics of the analyzed dynamical system.

Using this result in any PDE, the following equation is obtained:

$$\sum \frac{da_n}{dt}\phi_n = N\left(\sum a_n\phi_n, \sum a_n\phi_{nx}, \cdots, x, t\right) \tag{8}$$

There are a few possible basis functions, but for the case of the POD decomposition, the basis functions that have the orthonormality property will be applied. This property indicates that:

$$\langle \phi_n \ , \ \phi_m \rangle = \delta_{nm} = \begin{cases} 0 & n \neq m \\ 1 & n = m \end{cases} \tag{9}$$

where the term δ_{nm} is the Dirac function and $\langle \phi_n \ , \ \phi_m \rangle$ is the inner product, defined as:

$$\langle \phi_n \ , \ \phi_m \rangle = \int_{-L}^{L} \phi_n \phi_m^* \, dx; x \in [-L, L] \tag{10}$$

where * stands for complex conjugation, n is the number of rows and m is the number of columns of a matrix.

Accordingly, the PDE equation will be multiplied on both sides by ϕ_m and integrated over $\int_{-L}^{L}$:

$$\int_{-L}^{L} (\phi_m) \times \sum \frac{da_n}{dt}\phi_n = \int_{-L}^{L} (\phi_m) \times N\left(\sum a_n\phi_n, \sum a_n\phi_{nx}, \cdots, x, t\right) \tag{11}$$

Therefore, all the terms $\phi_n \times \phi_m$ will be set to zero and the terms $\phi_n \times \phi_m$ will be equal to 1, both due to the inner product property:

$$\frac{da_m}{dt} = \langle N \ , \ \phi_m \rangle; m = 1, 2, 3, \cdots, N \tag{12}$$

There are several approaches to solving the above equation, which aim at convergence of the equation. This can be achieved by carefully choosing the basis functions ϕ and the number of modes n. Therefore, we will consider the input dataset of the matrix **X** and the SVD decomposition:

$$\mathbf{X} = \begin{bmatrix} | & | & | & | \\ x_1 & x_2 & \cdots & x_m \\ | & | & | & | \end{bmatrix} \tag{13}$$

$$\mathbf{X} = \mathbf{U}\Sigma\mathbf{V}^T \tag{14}$$

In particular, regarding the POD decomposition, the SVD generates the matrix **U** from the input data, which has the dominant modes of the POD in its columns. The first dominant mode is in the first column and so on, which are orthonormal to each other. When analyzing the singular values of the Σ matrix, it is common to find that the first few principal modes accumulate almost all of the variation in the dynamic system. Therefore, only the first few columns of **U** are needed to reconstruct the input data matrix, which will have a smaller dimension than the initial one. Hence, it is possible to consider the truncated SVD decomposition:

$$\tilde{\mathbf{X}} = \tilde{\mathbf{U}}\tilde{\Sigma}\tilde{\mathbf{V}}^T \tag{15}$$

Briefly, the optimal POD basis functions are generated from a truncated SVD decomposition of the PDE. With this, it is possible to reshape the system dynamics into the best low-dimensional structure, which can be described as a function of the dominant modes, i.e. the most energetic ones:

$$\tilde{\mathbf{U}} = \phi = \begin{bmatrix} | & | & | & | \\ \phi_1 & \phi_2 & \cdots & \phi_r \\ | & | & | & | \end{bmatrix} \tag{16}$$

where r are the first truncated energy dominant modes of the matrix Ũ.

Most of the energy of the PDE dynamical system is concentrated in the first few modes of the POD, which reinforces the fact that few modes are needed to achieve an efficient accuracy during the reconstruction of the original matrix.

3. RESULTS

Each image processing presented previously was tested separately, which made it possible to visualize which denoising parameter was the most suitable for eliminating the greatest amount of noisy data. The experimental images filtered by separate image processing are represented below, as well as the selected optimal parameter.

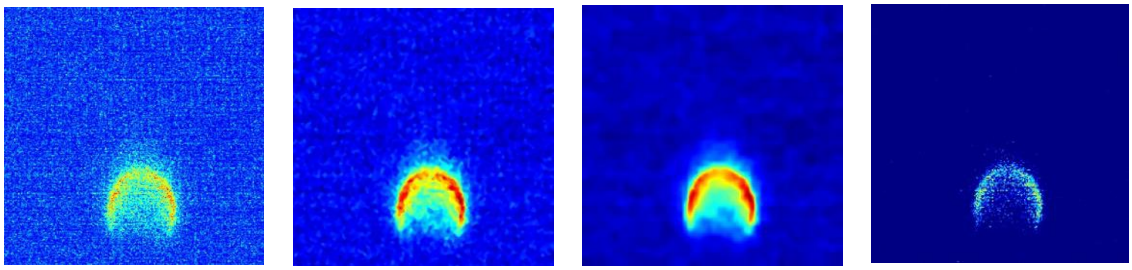

(a) (b) (c) (d)

Figure 2. Original image obtained from the experiment (a), Image processed by median filter with optimal denoising parameter 3×3 (b), by BM3D filter with optimal denoising parameter 25 (c), by threshold filter with optimal denoising parameter 35 (d). All images have size 256×256 pixels and 2000 frames per second.

The optimal parameters were selected so as not to eliminate relevant information from the experiment. If denoising parameters are used excessively, information is lost. Therefore, for each image processing analyzed, the optimal parameters are not redundant. Then, aiming to capture the largest possible number of POD dominant energy modes, image processing with the respective optimal filtering parameters were applied simultaneously to the experimental digital images of the oscillatory methane jet diffusion flames. This analysis is illustrated in the following images.

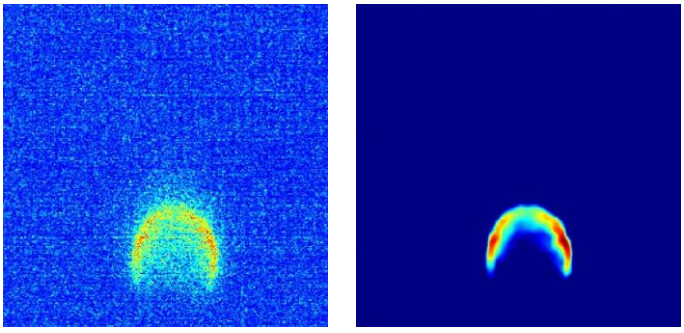

(a) (b)

Figure 3. Original experimental image (a), experimental processed image with the median filter with optimal denoising parameter 3×3, BM3D filter with optimal denoising parameter 25, threshold filter with optimal denoising parameter 35 (b). All images have size 256×256 pixels and 2000 frames per second.

With the simultaneous application of image processing and their respective optimal noise reduction parameters, it was possible to eliminate a large part of the previously existing noisy signals. This allowed a comparison to be made of the dominant modes resulting from the POD decomposition, before and after image processing. Therefore, we can say that the image processing applied to the images obtained by the experiment improved the result of the modal decomposition and, consequently, the obtaining of more dominant energy modes.

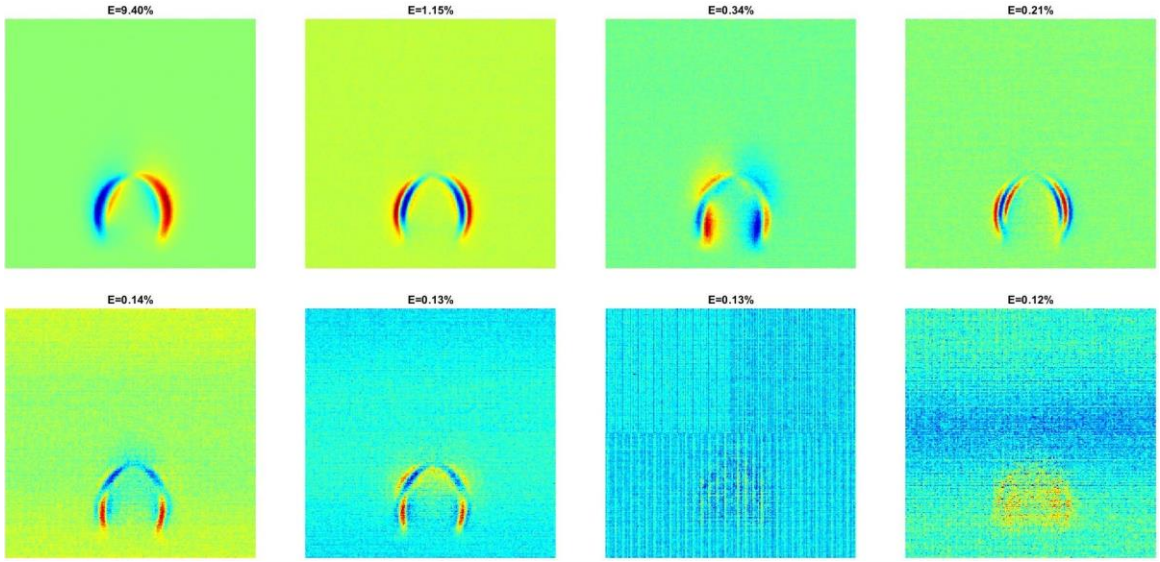

Figure 4. First eight dominant energy modes from the POD decomposition of the original images obtained from the experiment.

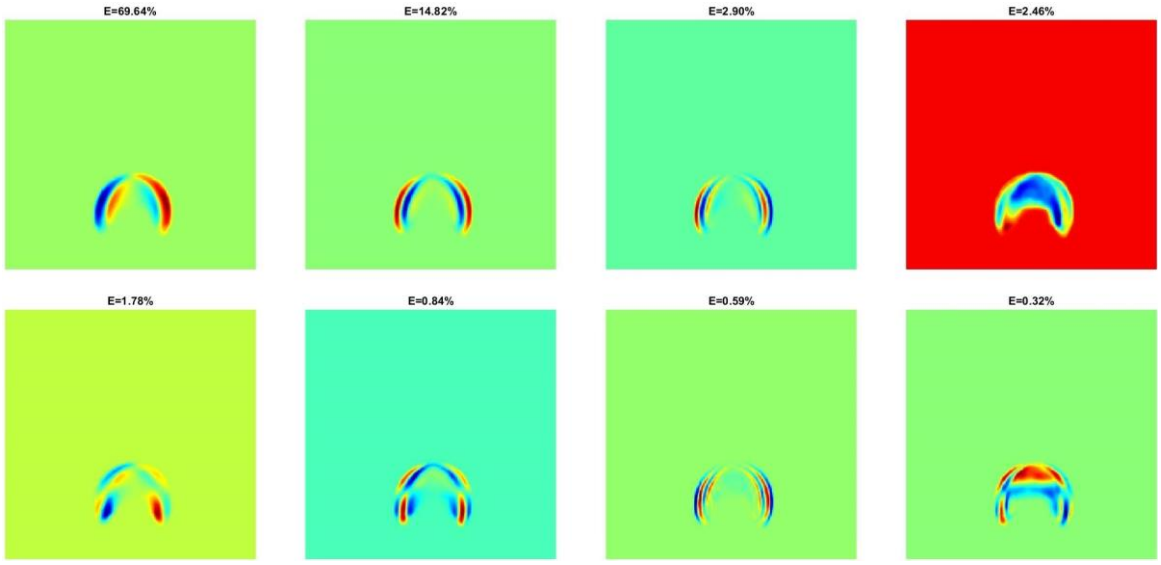

Figure 5. First eight dominant energy modes from the POD decomposition of the images processed of the experiment.

The dominant energy modes of the POD decomposition of the original images of the experiment accumulate only 11.62% of the total energy of the dynamic system of the diffusive flames. This percentage is not valid, as very limited energy was captured from the original system. Therefore, it is not possible using these dominant modes to describe the real dynamics of the system. Therefore, the POD decomposition was performed with the post-processed images of the flames. Analyzing the first eight dominant POD energy modes, it is possible to say that the modes accumulate 93.35% of the total energy of the methane jet flame dynamic system. This percentage of energy is valid, as it states that the modal decomposition captured almost all of the energy of the original dynamical system in its first eight dominant modes. Therefore, the phase portraits of the dominant energy modes of the original and processed images were generated, as illustrated below.

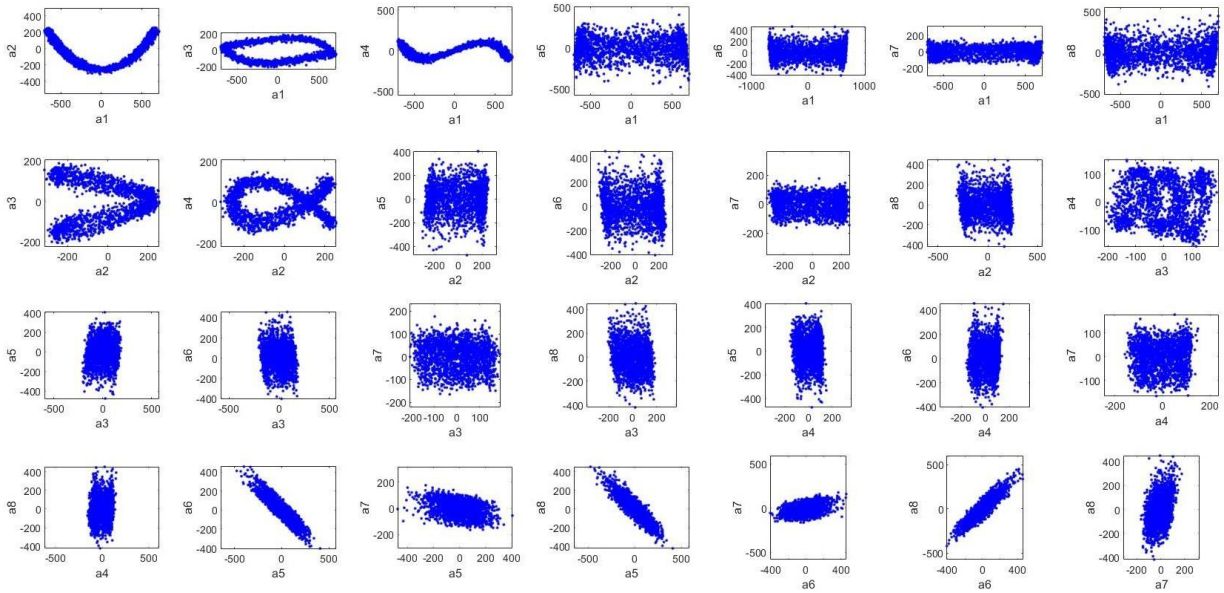

Figure 6. First eight 2D phase portraits of the dominant energy modes from the POD decomposition of original images obtained from the experiment.

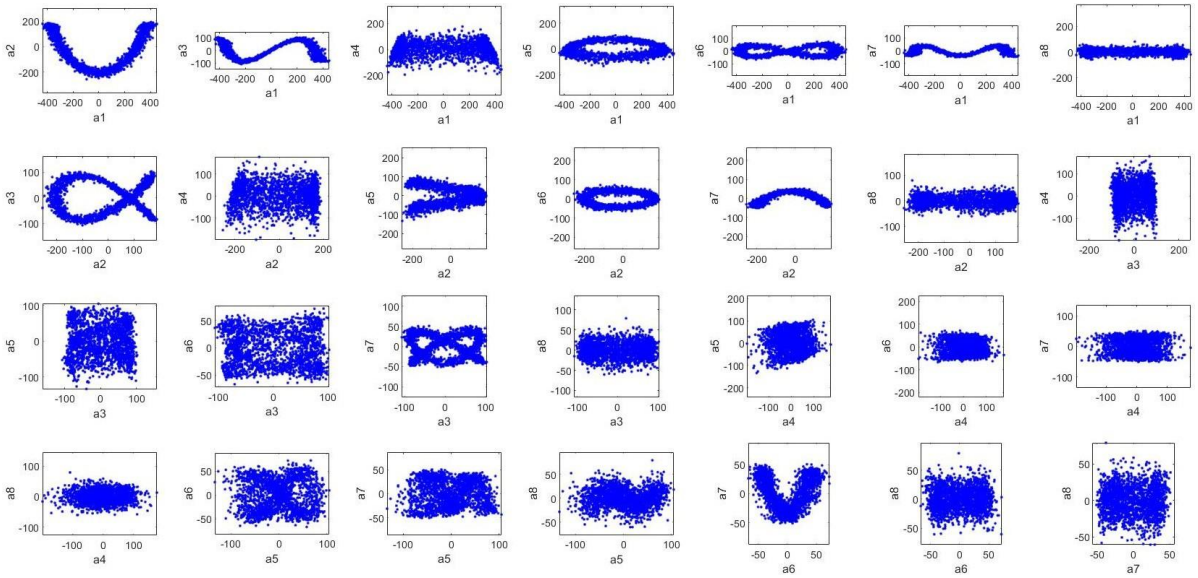

Figure 7. First eight 2D phase portraits of the dominant energy modes from the POD decomposition of the images processed from the experiment.

The 2D phase portraits of the dominant POD energy modes in the original images from the experiment are surrounded by noise and do not represent the real dynamics of the observed system. In regards to the processed images from the experiment, it can be seen that the phase portraits of the dominant energy modes are valid and have well-defined trajectories. However, for the later modes, such as the seventh and eighth, there is still a lot of noise in the trajectories. Therefore, for the original and processed images of the experiment, an analysis was performed up to the sixth energy mode and its trajectories in 3D space, as illustrated below.

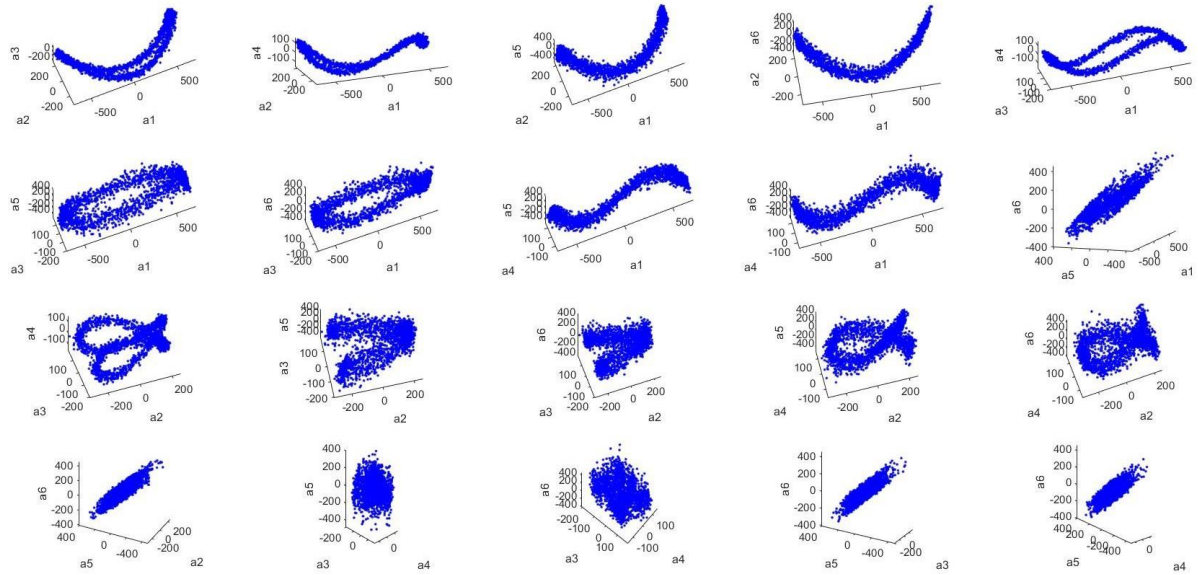

Figure 8. First six 3D phase portraits of the dominant energy modes from the POD decomposition of the original images from the experiment.

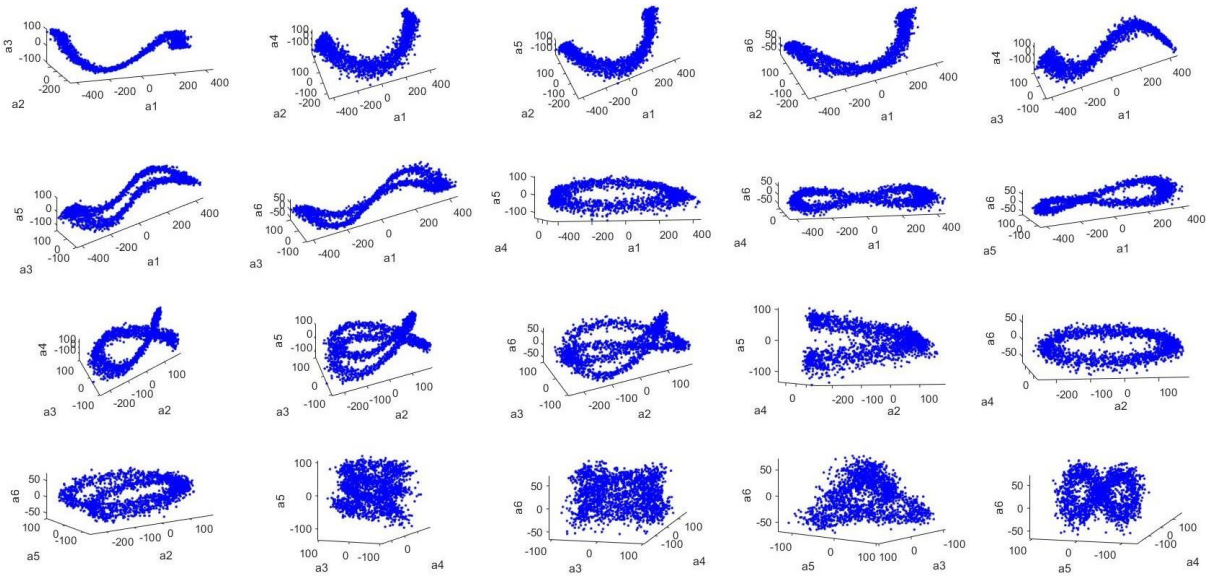

Figure 9. First six 3D phase portraits of the dominant energy modes from the POD decomposition of the images processed from the experiment.

4. CONCLUSIONS

As a consequence of the image processing performed, it was possible to capture dominant energy modes of the POD decomposition, as well as the respective phase portraits. However, just analyzing the dominant energy modes is not enough to say whether the image processing performed was adequate. For this reason, phase portraits of these modes were generated, both 2D and 3D. Observing the phase portraits, it is possible to affirm that the further ahead the energy modes are, the more noise they present. Therefore, only the first six modes and the 3D phase portraits were considered. In these portraits, most of the trajectories are defined, but there are still trajectories that are dominated by noise, making it not possible to visualize the analyzed dynamics. Therefore, for future work, new image processing will be applied to images obtained from the oscillatory methane jet diffusion flames experiment, which will enable greater capture of trajectories defined in the phase portraits. With increased generation of phase portraits and subsequent capture of POD energy modes, a reduced order model for the flames can be developed.

5. ACKNOWLEDGEMENTS

The authors would like to thank the MAE Department at UCLA, essentially Professor Ann R. Karagozian and Andres Vargas, for the collaboration in obtaining the experimental data for this work.

6. REFERENCES

Sim, H. S., Vargas, A., Dongchan, D. A. Karagozian, A. R., 2020. *Laminar Microjet Diffusion Flame Response to Transverse Acoustic Excitation*, Combustion Science and Technology, doi: 10.1080/00102202.2020.1726897.

Lumley, J. L., 1967. *The structure of inhomogeneous turbulent flows.* Atmospheric turbulence and radio wave propa-gation.

Beltrami, E., 1868. *Saggio di Interpretazione della geometria non-Euclidean (Essay on the interpretation of non-Euclidean geometry)*, Giornale di Matematiche vol. VI, p. 284-322. Beltrami's Works, Vol. I, pp.374–405. French translation: Essai d'interpr´etation de la géométrie noneuclidienne, Trad. J. Houel, Annales scientifiques de l'Ecole Normale Supérieure, Sér. 1, Tome VI 1869, p. 251-288. English translations by J. Stillwell, in [56] pp. 7–34.

Jordan, C., 1876. *Mémoire sur les covariants des formes binaires*. Journal de Mathématiques Pures et Appliquées, Serie 3, Volume 2, pp. 177-232.

Tukey, J. W., 1971. *Exploratory Data Analysis*, Addison-Wesley, Reading, MA.

Dabov, K., Foi, A., Katkovnik, V., 2007. *Image denoising by sparse 3D transform-domain collaborative filtering*. IEEE Transactions on Image Processing, 16(8), 2080-2095.

Dabov, K., Foi, A., Katkovnik, V., Egiazarian, K., 2009. *Collaborative Filtering for Noise Reduction in Synthetic Aperture Radar Images*. IEEE Transactions on Image Processing, 18(5), 1241-1250. DOI: 10.1109/TIP.2009.2015472

Dabov, K., Foi, A., Katkovnik, V., Egiazarian, K., 2009. *Collaborative Filtering for Noise Reduction in Synthetic Aperture Radar Images*. IEEE Transactions on Image Processing, 18(5), 1241-1250. DOI: 10.1109/TIP.2009.2015472

Gonzalez, R. C., Woods, R. E., Eddins, S. L., 2020. *Digital Image Processing Using MATLAB*. Gatesmark Publishing.Gonzalez, R. C., Woods, R. E., 2018. *Digital Image Processing*. 4th edition. Pearson Publishing.

Otsu, N., 1978. *A threshold selection method from gray-level histogram*. IEEE Transactions on Systems, Man, and Cybernetics.

Lebrun, M., 2012. *An Analysis and Implementation of the BM3D Image Denoising Method*, Image ProcessingOnline2, 175–213.

Parker, J. R., 2011. *Algorithms for Image Processing and Computer Vision*. Wiley Publishing, 2nd edition.

Lee, J. S., 1980. *Digital Image Enhancement and Noise Filtering by Use of Local Statistics*, in IEEE Transactions onPattern Analysis and Machine Intelligence, vol. PAMI-2, no. 2, pp. 165-168, doi: 10.1109/TPAMI.1980.4766994.

Brunton, S.L., Kutz, J.N., 2018. *Data-Driven Science and Engineering: Machine Learning, Dynamical Systems, andControl*. Cambridge University Press.

Kutz, J. N., 2013. *Data-Driven Modeling Scientific Computation: Methods for Complex Systems Big Data*, Oxford Univ. Press, New York.

Kutz, J. N., Brunton, S. L., Brunton, B. W., and Proctor, J. L., 2016. *Dynamic Mode Decomposition: Data-Driven Modeling of Complex Systems*, SIAM, Philadelphia, PA.

LeGresley, P. A., 2005. *Application of Proper Orthogonal Decomposition (POD) to Design Decomposition Methods*,Ph.D. Thesis, Stanford University, Stanford, CA.

Cordier, L., and Bergmann, M., 2008. *Proper Orthogonal Decomposition: An Overview*, Lecture Series 2002-04, 2003-03 and 2008-01 on Post-Processing of Experimental and Numerical Data, Von Karman Institute for Fluid Dynamics, VKI, 2008, p. 46.

Noack, B. R., Morzynski, M., and Tadmor, G. (eds.), 2011. *Reduced-Order Modelling for Flow Control*, Springer, New York.

Schmid, P. J. Sesterhenn, J. L., 2008. *Dynamic mode decomposition of numerical and experimental data*. In Bull. Amer. Phys. Soc., 61st APS meeting, p. 208. San Antonio.

Tu, J. H., Rowley, C. W., Luchtenburg, D. M., Brunton, S. L., and Kutz, J. N., 2014. *On Dynamic Mode Decomposition: Theory and Applications*, Journal of Computational Dynamics, Vol. 1, No. 2, pp. 391–421. doi:10.3934/jcd

7. RESPONSIBILITY NOTICE

The authors are solely responsible for the printed material included in this paper.